Nanoparticle aggregation behaviour in polymer nanocomposites: bulk vs. thin films

2010 J. Phys.: Conf. Ser. 247 012046

(http://iopscience.iop.org/1742-6596/247/1/012046)

Journal of Physics: Conference Series **247** (2010) 012046 doi:10.1088/1742-6596/247/1/012046

Nanoparticle aggregation behaviour in polymer nanocomposites: bulk vs. thin films

Him Cheng Wong and Joao T Cabral[1]

Department of Chemical Engineering, Imperial College London, SW7 2AZ.

Email: j.cabral@imperial.ac.uk

Abstract. We report on the stability and cluster formation in C_{60} fullerene-polystyrene mixtures, using a combination of small angle neutron scattering, optical and atomic force microscopy. Bulk nanocomposites are found to be stable for C_{60} loadings up to 1-2% mass fraction in PS of M_w = 270 kg/mol and approximately 160°C. At larger fullerene concentration, the coherent scattering intensity grows with time, within 10s of min, and is well described by an asymptotic relationship with rate compatible with Arrhenius temperature dependence. The nanocomposite structure can be described by fractal scattering with a broad range of dimensions D_f ~1.85-2.4 and polydisperse fractal sizes, up to hundreds of nm, depending on annealing temperature and time. Confinement in thin films of tens to hundreds of nm is shown to result in well-defined surface topographies, ranging from isolated clusters to percolated spinodal-like undulations with tuneable wavelength and amplitude. These results provide insight into the control of dispersion and self-assembly of nanoparticles in polymer matrices and thus their exploitation in functional materials, including organic photovoltaics and thin film coatings.

1. Introduction

The introduction of trace amounts of nanoparticles (NPs) in polymers (P) can significantly enhance and tune their mechanical, electrical and thermal properties. The performance of these so-called polymer nanocomposites (PNCs) is however largely governed by the dispersion of the NP, which remains "the greatest stumbling block to the large-scale production and commercialisation of nanocomposites" [1]. While well dispersed NPs can enhance the material's mechanical properties and processibility [2], NP segregation can also be advantageous, for example in controlling thin film stability [3-5] and morphology in advanced applications including photovoltaics [6]. Composites based on conducting polymers and fullerene (C_{60}) derivatives are particularly attractive for applications in flexible electronics, light-emitting displays, and photovoltaics since the discovery of photoinduced electron transfer between conducting polymers (donor) and C_{60} (acceptor) [7]. Clustering of C_{60} in selected polymer matrices [8, 9] and solvents [10, 11] has been well documented, as well as in the pure solid state, where C_{60} clusters with aggregation number of up to 55 were found by mass spectrometry [12]. Systematic studies are however needed to understand fullerene association in polymer matrices in detail, and thus the effect of processing, in order to explore its potential as performance enhancing fillers.

[1] To whom any correspondence should be addressed.

Particle aggregation studies can be carried out both in direct (or real) and reciprocal spaces, with well defined advantages and limitations. Real space studies involve detailed analysis of microscopy images and are often limited by image overlapping of 3-dimensional structures, lack of contrast, and non-representative local sampling. As a complementary technique to microscopy, small angle scattering (SAS) measures the spatial correlations in a mesoscopic range, typically from 1-1000 nm, depending on the radiation and angle of scatter. SAS is one of the best established techniques to elucidate the structural features of NP in nanocomposites such as its radii of gyration (R_g), shape, surface-to-volume-ratio, aggregation nature and size distribution. Sorensen et al. [13] and Rieker et al. [14] have adopted small angle X-ray scattering to characterise the fractal nature of carbon black aggregates, while structural information of C_{60} NP in benzene solution has been studied extensively using static and dynamic light scattering [10]. A recent study by Narayanan et al. [15] combined transmission electron microscopy and ultra small angle X-ray scattering to study the nanostructural features of fumes silica NPs in poly(vinyl acetate), fully characterising the size distribution and fractal nature of the silica NP.

In this paper, we investigate the aggregation /association behaviour of C_{60} NP in bulk polystyrene (PS) and compare it with its thin film counterpart, using reciprocal and real techniques, respectively. In the first part, we probe the structural information of C_{60} NP in a bulk hydrogenous polystyrene matrix using SANS. We compute the time evolution of the scattering intensity as a function of wavenumber q to study the NP aggregation as a function of particle loading and annealing temperature. The growth rate of the scattering intensity is then fitted to an empirical kinetic equation in order to determine the growth kinetics of the aggregation process. We then obtain fractal exponents for nanocomposites with representative particle concentration and annealing temperatures and times. Finally, a combination of optical microscopy (OM) and atomic force microscopy (AFM) is employed to elucidate the association of NPs in thin films of entangled PS-C_{60} annealed above glass transition temperature (T_g). Confinement in thin films (10s-100s of nm) breaks the symmetry of bulk association and leads to clustering of fullerenes in a spinodal pattern under specific conditions, providing a route to tuneable, functional particle-polymer structures [16].

2. Experimental section

2.1. Materials used and sample preparation

Bulk and thin film samples of PS-C_{60} nanocomposites were prepared using rapid precipitation and spin coating method, respectively, following procedures which were reported elsewhere [16, 17]. In short, bulk composites were prepared by separate dissolution of polymer and nanoparticle in toluene dilute solution, ultrasonication, mixing and further sonication and finally co-precipitation in a 5-fold excess of methanol (non-solvent). After drying under full vacuum at 100°C for 3 days, the resulting nanocomposite fibre was hot-pressed at 150°C for 6 min, below the agglomeration threshold limit [17], into 0.33 mm thick, 16 mm diameter disks; three individual films were then stacked and wrapped in aluminium foil, resulting in approximately 1 mm thickness (and 60% neutron transmission). Neutron contrast (neutron scattering length density) of C_{60}, hydrogenous PS and deuterated PS is respectively 5.7, 1.41 and 6.42 $\mu Å^{-2}$. To maximize contrast, we opt to study C_{60} association in hydrogenous polymer matrix, which requires careful incoherent background subtraction.

Thin films were spun cast onto silicon wafers (with a 2 nm silicon oxide layer) from ultrasonicated dilute toluene solutions of 0.1-2.5 % mass fraction to obtain film thicknesses between 10 to 150 nm. Spun cast thin film samples were dried at room temperature for at least one day prior to annealing.

Fullerenes were purchased from MER Corp. (99+% purity) and were used as received. Polystyrene was obtained from BP Chemicals and re-precipitated into a five-fold excess of non-solvent methanol and characterised by Gel Permeation Chromatography (GPC), yielding molecular mass M_w = 270 kg/mol and polydispersity index PDI = 2.3, thus radius of gyration R_g~14 nm.

2.2. Small angle neutron scattering

SANS experiment were carried out at two small-angle neutron scattering diffractometers: (a) LOQ (ISIS, Oxfordshire), a fixed-geometry instrument at the pulsed source with the sample-detector distance of 4 m which translates to a wide wavenumber range (0.009 $Å^{-1} < q < 0.249$ $Å^{-1}$) due to the polychromatic nature of the incident beam (wavelength 2 Å to 10 Å); (b) PAXE at the (Laboratoire Léon Brillouin, Saclay) configured to λ = 15 Å and sample detector distance of 5.11 m, yielding a wavenumber window between 0.0033 $Å^{-1}$ and 0.048 $Å^{-1}$. SANS data was calibrated using a primary standard (isotopic polymer blend) and the direct beam. The corresponding length scale window accessible by combination of the two instruments is approximately 2 nm < d < 30 nm.

In order to study C_{60} aggregation kinetics, 'fresh' (i.e. as pressed) nanocomposites are kept below T_g. where the structure is frozen, and then rapidly 'jump' to the experimental temperature (above T_g) while the synchronised time-resolved SANS measurement is triggered. In this work, we have employed a custom-made neutron scattering 'kinetic' cell, depicted in Figure 1. The cell consists of a brass pre-heating block, an experimental block with quartz windows and 45° exit cone, and a thin brass sample carrier which moves the sample quickly (within 2 s) between the two blocks.

In addition to time-resolved measurements, bulk PS-C_{60} samples were also measured quiescently: (a) 'unannealed' (as melt pressed) samples; (b) samples which were annealed ex-situ in vacuum oven at 160 ± 10°C for 12 h ('ex-situ annealed' samples). The latter samples are measured ex-situ while the unannealed samples were measured while annealing in-situ. Typical acquisition times were 20 min for quiescent specimens and 10 min for time-resolved measurements.

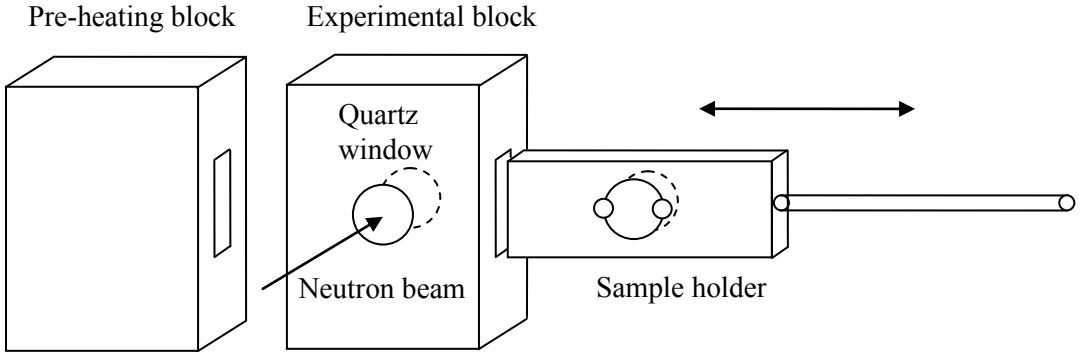

Figure 1. Schematic of the 'Temperature Jump' neutron kinetics scattering cell, depicting the pre-heating and experimental ovens and motorised sample holder. [18]

2.3. Optical and atomic force microscopy

The morphology of polymer nanocomposites thin films was studied in-situ using a custom made hot stage mounted on a reflection optical microscope (Olympus BX41M) equipped with a CCD camera (Adimec 1000m) controlled by LabVIEW. The surface topography was further characterized by tapping-mode AFM (Innova, Veeco) using super-sharp TESP-SS probes. The data was analysed by fast-Fourier Transform and radial averaging (ImageJ, NIH, USA) and NI Vision assistant to obtain particle sizes and in-plane structure periodicity.

3. Results and discussion

A systematic C_{60} aggregation study in PS matrix as a function of C_{60} loading and annealing temperature using SANS was conducted and representative results are shown in Figure 2. After annealing at 180˚C for a short period of time (14 min), excess forward scattering can be observed for samples containing more than 2% mass fraction of C_{60}. Scattering of 1% PNC sample and neat PS is identical, indicating good C_{60} dispersion below 2%.

In the second series of experiment, we study the effect of annealing temperature on the dispersion of C_{60} NPs at a constant 2% mass fraction. Figure 2(b) demonstrates that annealing temperature plays an important role in governing the NP aggregation process and indicates a sharp onset of cluster-formation between 160˚C and 180˚C. In short, the experiments indicate a NP aggregation threshold concentration at 1-2% and temperature above 160˚C.

We have previously conducted a complementary aggregation study using differential scanning calorimetry (DSC) [17, 19]. C_{60} is shown to increase the T_g of PS by up to 4˚C at approximately 4%.Upon annealing above the threshold temperature (T^*), the T_g of the nanocomposites which exceed the threshold concentration (ϕ_c) will recover towards a lower plateau value. We associate this T_g recovery to NP agglomeration, thereby decreasing surface area in contact with polymer matrix. It is observed that the onset of T_g deviation between 'fresh' and 'annealed' samples occurs between 1-2% mass fraction (ϕ_c) (Figure 3(a)) and above 160˚C (T^*) (Figure 3(b)), in agreement with previous [17] and current SANS results which show significant excess forward scattering beyond the same threshold. The good agreement between our DSC and SANS results indicates that the T_g is a suitable gauge for the extent of dispersion of NP composites [17].

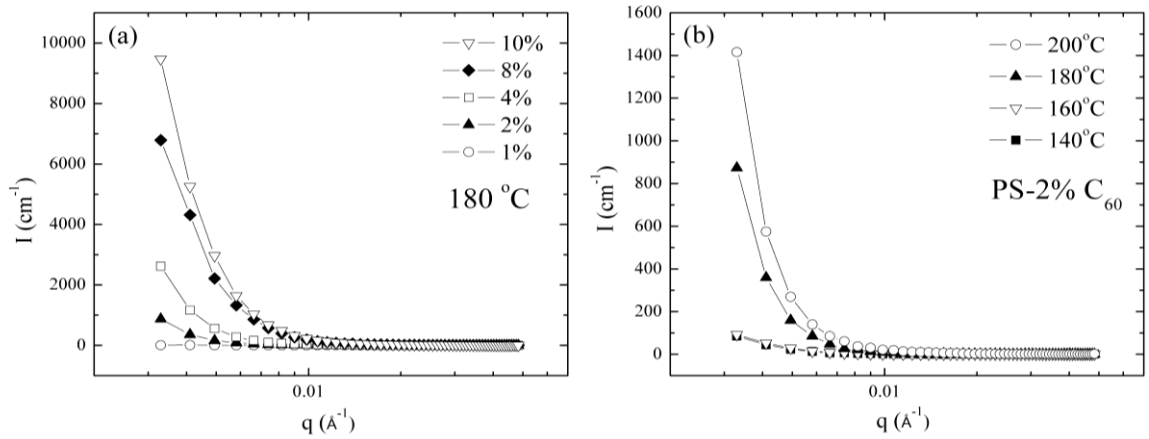

Figure 2. (a) SANS spectra of bulk polystyrene (PS) nanocomposites containing C_{60} mass fractions ranging from 1% to 10%, annealed at 180°C for constant time 14 min (b) effect of annealing temperature on PS-2% C_{60} at constant time 14 min.

3.1. NP aggregation kinetics in bulk

The time dependence of the scattering intensity of a PS-2% C_{60} composite annealed at 180˚C as a function of wavenumber is shown in Figure 4(a). This representation is a temporal cross section of the 2% specimen in Figure 2(a). The intensity rises rapidly with time and, in the q-range examined, the growth kinetics can be approximated to an asymptotic behaviour where $I_0 = I(t=0)$ and $I_\infty = I(t\rightarrow\infty)$ are the scattering intensity before and after the annealing period; $K(q)$ is the growth rate [s^{-1}]:

$$I(q,t) = I_0 + (I_\infty - I_0)(1 - e^{-K(q)t}) \qquad (1)$$

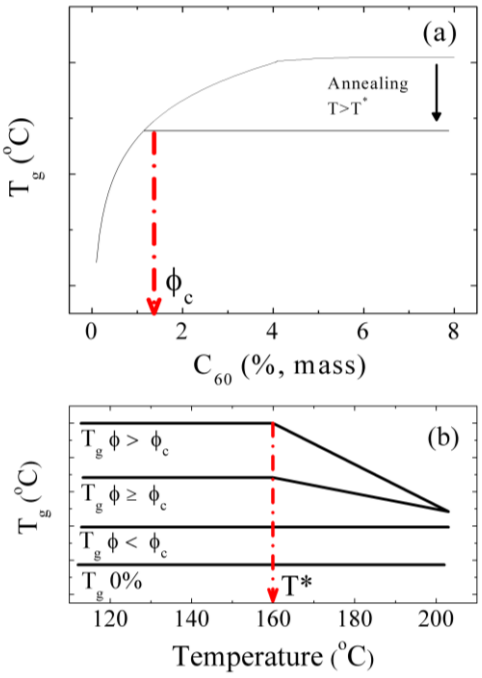

Figure 3. Schematics illustrating the effect of thermal annealing on the glass transition temperature (T_g) of the nanocomposites as a function of (a) C_{60} loading and (b) annealing temperature. DSC agrees remarkably well SANS in determining agglomeration threshold ϕ_c and T^*.

K(q) varies slowly with q across the wavenumber range studied, with up to 30% changes from the highest and lowest q, as shown in Figure 4(a). Next, we concentrate on the intensity at the lowest q accessible for comparison purposes between composites of different C_{60} loading. Figure 4(b) plots the time dependence of the scattered intensity from nanocomposites with different C_{60} concentrations annealed at 180˚C. As expected, scattering intensity of 1% sample shows weak time dependence in comparison with the 2% specimen.

Above the threshold aggregation concentration, at constant annealing temperature of 180˚C the NP growth at 4% loading is faster relative to 2%, as evidenced by the slight increase in growth constant ($K \approx 0.07\ s^{-1}$ from $K \approx 0.06\ s^{-1}$) and shorter annealing time (20 min from 50 min) to reach 95% of the 'plateau' value. Further work is necessary to elucidate how the NP aggregation kinetics changes with annealing temperature in samples exceeding the threshold concentration. The scattering intensity with for 8% and 10% does not change with time, as shown in Figure 4(b), indicating that the specimens are agglomerated at the outset and the 'saturation' state is reached even before annealing.

At 2% mass fraction, which is the upper limit of the aggregation threshold, the kinetics of the C_{60} NP aggregation is also investigated as a function of annealing temperature (Figure 4(c)). The time evolution of the scattering intensity for each annealing temperature is well described with the asymptotic relation above. The growth constant K for each annealing temperature is obtained from the fit and plotted against inverse temperature, as shown in the inset of Figure 4(c). The growth constant is predictably decreasing with annealing temperature and can be described by an Arrhenius temperature dependence, as expected at high temperatures (well above T_g). Each annealing temperature appears to have its own 'plateau' value, which would imply that not only the clustering kinetics but also the asymptotic morphology depends on temperature. Further work is necessary to extend the time window and intermediate temperature range, as the matrix viscosity varies rapidly with T according to WLF relationship.

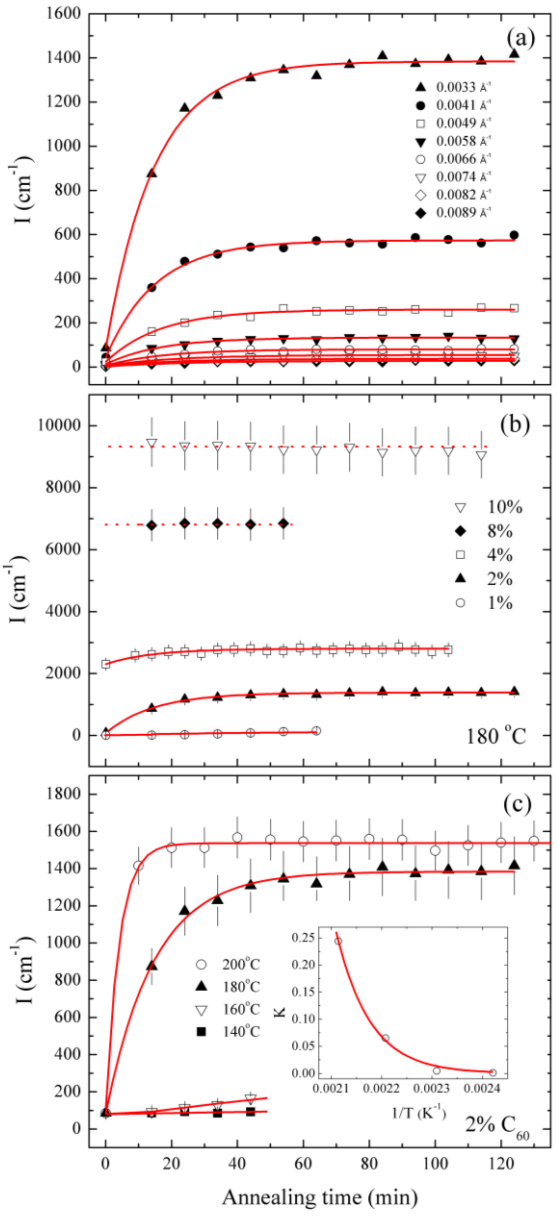

Figure 4. (a) Growth kinetics of C_{60} aggregates in bulk sample containing 2% mass fraction of C_{60} under in-situ thermal annealing at 180˚C, expressed in terms of different q values. The q value that we adopt in subsequent kinetics study (b and c) is 0.0033 $Å^{-1}$. Bulk C_{60} aggregation kinetics as a function of (b) C_{60} mass fraction under isothermal annealing at T = 180˚C and (c) annealing temperature for sample containing 2% mass fraction of C_{60}. Inset in (c) shows the Arrhenius temperature dependence of the K constant. Red solid lines are best fits according to Eq. (1) while red dash lines are linear guide-to-the-eye.

At short times, the intensity growth with time can be described by both an asymptotic relationship (Eq. (1)) and a logarithmic function [17]. Indeed, the Maclaurin second order polynomial approximation of $(1-e^{-x})$ and $\ln(1+x)$ is identical. However, at longer times, Eq. 1 appears to describe the intensity growth data more accurately and is hence adopted in this work. Further it has a clearer physical meaning as it predicts an asymptotic structure at long times, as large clusters are formed, instead of continuous growth.

3.2. NP fractal dimension

(Nano)particle aggregates may form 'statistically self-similar' structures within a range of lengthscales and are thus treated as fractals [20]. Numerous soft matter systems such as linear or branched polymers, colloids and nanoparticles exhibit fractal behaviour. The scattering intensity I (q) can be related to the scattering vector q via the following power-law equation:

$$I(q) \sim q^{-D_f} \qquad (2)$$

where D_f is called fractal or Hausdorff dimension which can be extracted as the negative slope of the scattering data plotted in log-log scale. Several growth mechanisms that lead to fractal aggregates have been proposed based on computer simulations. Witten and Sandler [21, 22] first proposed the diffusion limited aggregation (DLA) growth model which involves an immobilized growth site and one diffusing particle which randomly walks from a distant lattice point until it collides with the stationary growth site. The repetition of this process generates remarkable self-similar fractal structures. DLA is a fast aggregation process which is only limited by the diffusion time of the particle and the resulting D_f of the structure in two and three dimensions is ~ 1.7 [21] and ~ 2.5 [23], respectively. Another model of fractal formation involves multiple aggregations of relatively monodisperse particles. This so-called cluster-cluster (DLCA) aggregation proposed by Jullien and co-workers and Meakin [24, 25] is in contrast to the exclusive small - large cluster growth of DLA. Two particles next to each other will aggregate and continue to diffuse, becoming cluster sites themselves to form larger fractal structures, with D_f ~ 1.8 – 2.05 in three dimensions [26].

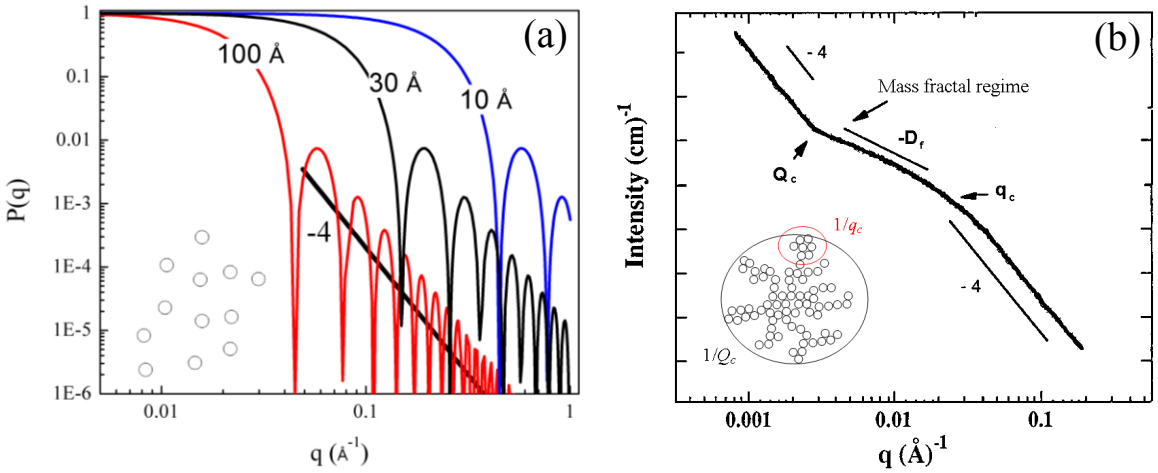

Figure 5. (a) Computed form factor of a sphere with radius r with respect to wavenumber q. Note the Porod regime towards high q value has -4 q dependence. (b) Typical scattering pattern from fractal system (See text below).

There are generally 3 power-law regimes in typical scattering data from fractals (Figure 5(b)). At low- q, the upturn in scattering intensity is attributed to scattering from the fractal agglomerates which gives a power-law exponent of -4 [13]. Whereas scattering from the surface of the individual particle happen at the high- q regime which is also known as the Porod power law regime (slope of -4 is again observed) (Figure 5(a)). In between these two boundaries, at the 'intermediate' q range, lies the fractal regime which has a smaller D_f that describes the type of fractals in the system. The individual primary aggregate size is inversely proportional to the q value (via 1/d) at the crossover point q_c from the fractal regime to Porod regime at high q whereas another crossover value Q_c indicates departure from fractal regime to agglomerate regime at low q-regime, corresponding to the size of an agglomerate.

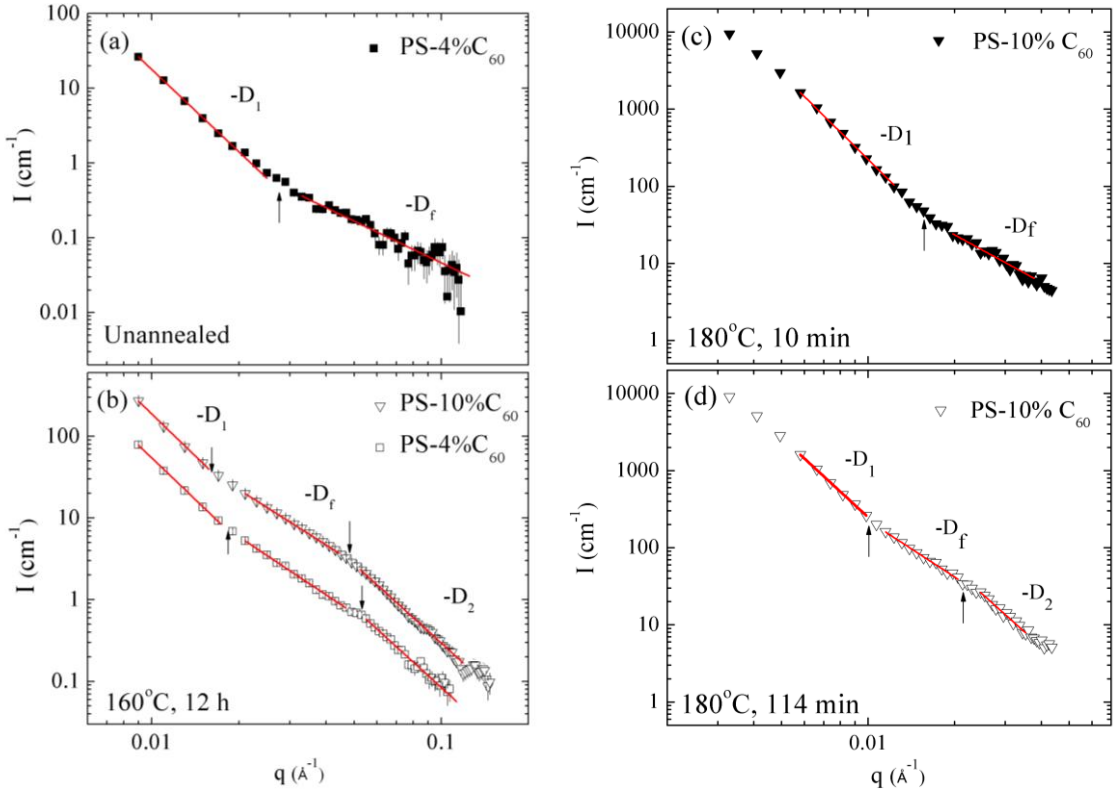

Figure 6. Selected log-log plots of SANS spectra of bulk PS-C_{60} nanocomposites. (a) PS-4% C_{60} composite before annealing and (b) PS-4% and 10% annealed ex-situ at 160°C for 12 h, measured at LOQ. PS-10% C_{60} annealed in-situ at 180°C measured after (c) 10 min and (d) 114 min (PAXE, LLB). Red solid lines are fits to a power-law equation, giving the mass fractal exponent D_f; arrows indicate crossover points Q_c and q_c. The exponents and the crossover points Q_c and q_c are tabulated in Table 1.

Upon subtraction of the incoherent background, normalised by the mass of the PS alone, the coherent scattering from bulk nanocomposites with loading exceeding 2% C_{60} are well described by a power law, with exponents D_f of 1.85 to 2.4 (Figure 6). Samples with lower C_{60} loading and typical acquisition times of 20 min do not provide enough statistics to yield permit a reasonable estimate of D_f. Results for 4 and 10% C_{60} loading are shown in Figure 6 with various thermal treatments. We first consider a relatively low annealing temperature of 160°C in Figures 6(a), (b): the unannealed PS-4% composite (Figure 6(a)) does not show a q_c; upon 12 h annealing (Figure 6(b)), both 4% and 10% specimens show a distinct q_c within the measured q-window. The latter shows lower Q_c and q_c crossover points, as expected for larger fractal structures and primary aggregates. Separately, we consider the effect of higher temperature annealing at 180°C on PS-10% C_{60} composites: Figure 6(c) and (d) correspond to annealed times of 10 min and 114 min at 180°C. With time, the structure factor shifts towards low q, corresponding to a reduction in Q_c and the emergence of a q_c within the observed window. However, the Q_c and q_c values in (d) are still lower those on (b) indicating that the extent of agglomeration is greater after 2 h at 180 than 12h at 160°C. In addition, the comparable Q_c values for fresh and annealed PS-10% C_{60} samples at 160°C (12 h) and 180°C (2 h) suggests the composites cluster from the outset and their structure varies slowly thereafter. The summary of q_c, Q_c and D_f are presented in Table 1.

The primary cluster size ($1/q_c$) is estimated from the high- q fractal cutoff q_c as ranging from 2-5 nm (commensurate with C_{60} size of 1 nm). The apparent fractal sizes estimated from $1/Q_c$ are of the order of 10s of nm. However, agglomerates larger than 250 nm have been observed by TEM on bulk

PS-C_{60} nanocomposites [27] and micron-sized clusters are visible in thin films (10-100nm) upon thermal annealing (discussed below). Such dimensions are is outside the spatial range of the present SANS study. The discrepancy of fractal sizes suggests that these 'secondary' aggregates (size ~ $1/Q_c$) further associate to form micron-sized agglomerates in a fractal manner, resulting in polydisperse particle size distributions. Based on DSC measurements, we have indeed proposed earlier that aggregates become polydisperse beyond 1% mass fraction of C_{60}. Future work should cover such large lengthscales by USANS and USAXS and size distribution analysis accessible based on relevant fitting models. Small-angle light scattering is unfeasible due to low light transmission above 0.1% C_{60}.

Table 1. Exponents from power law fits and crossover points of SANS data shown in Figure 6.

Sample	D_1	D_f	D_2	Q_c [Å^{-1}]	q_c [Å^{-1}]
Unannealed PS-4% C_{60} LOQ	3.66	1.85	-	0.03	-
PS-4% C_{60} LOQ (160±10°C, 12 h)	3.39	2.36	3.22	0.018	0.053
PS-10% C_{60} LOQ (160±10°C, 12 h)	3.42	2.2	3.21	0.016	0.049
PS-10% C_{60} PAXE (180°C, 10 min)	3.69	2.04	-	0.014	-
PS-10% C_{60} PAXE (180°C, 114 min)	3.44	2.4	3.34	0.01	0.021

The fractal dimensions obtained agree well with that excepted for mass fractal aggregates. However, the broad range of fractal dimensions from 1.85 to 2.4 means their growth mechanisms could follow both the diffusion limited aggregation (DLA) and diffusion limited cluster-cluster aggregation (DLCA) growth model. The slight higher fractal dimension of annealed 4% and 10% sample (D_f = 2.2 to 2.4) could be rationalized with increase in polydispersity at high C_{60} loading [17] or branching of the mass-fractal aggregates [15]. The latter explanation is in agreement with the DLA growth model as the fast and Brownian diffusion [28] of NP is more likely to be colliding with a branched arm than the center of the cluster site. The lower D_f of 2.04 for the 10% sample in the early stage of annealing could suggest that clusters are less branched.

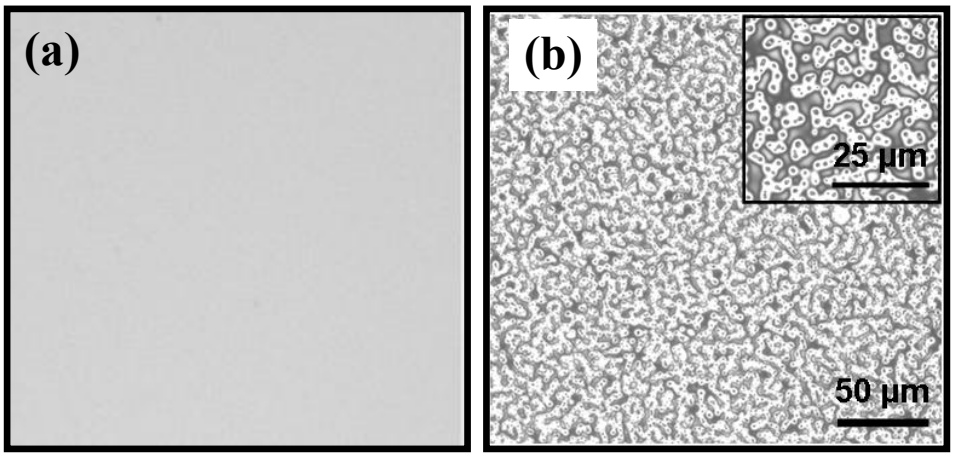

Figure 7. Optical micrograph of (a) neat PS and (b) PS thin film containing 5% mass fraction of C_{60} (thickness [h] = 150 nm) after annealing for 30 min at 180˚C. Upon annealing, the neat film remains uniform while the filled counterpart shows a spinodal clustering morphology, reported in [16].

Nanoparticle aggregation under 2D thin film confinement

Spatial confinement in thin films is expected to break the fractal growth symmetry in the bulk and possibly result in the coupling of lengthscales. Further, the glass transition temperature of polymers is known to be altered due to the confinement in nanopores and thin polymer films, and depends strongly on surface interactions. [29, 30] Following our investigation of NP in bulk nanocomposites, NP clustering in the polymer nanocomposite thin film counterpart is investigated in real space using optical and atomic force microscopy.

Figure 7 compares the lateral morphology of a high M_w (270 kg/mol) PS thin film (thickness [h] = 150 nm) and its nanocomposite (5% mass fraction of C_{60}) counterpart upon annealing at 180°C for 30 min. While the neat film remains uniform and stable within the experimental time scale of up to 10 hours, C_{60} NP in the nanocomposites thin films aggregates in a spinodal pattern within minutes (see inset of Figure 7(b)). Decreasing C_{60} loading (2wt%) results in nucleation and growth of clusters; these may percolate at long annealing times(>days) while above a threshold concentration exceeding 2%, forming interconnected spinodal-like morphologies, as depicted in Figure 7(b).

AFM topography scans of annealed nanocomposites thin films (Figure 8) shows that the films do not dewet from the substrate. Instead, C_{60} aggregates grow and are covered by a PS top layer (with lowest surface energy) forming peak-like structures, resulting an undulating surface topography that develops with time, with amplitude reaching between 100 - 200 nm. Selective dissolution of PS in the sample using tetrahydrofuran (THF) reveals that the micron-sized C_{60} aggregates (insoluble in THF) are anchored on the substrate, retaining their spinodal morphology (data not shown here).

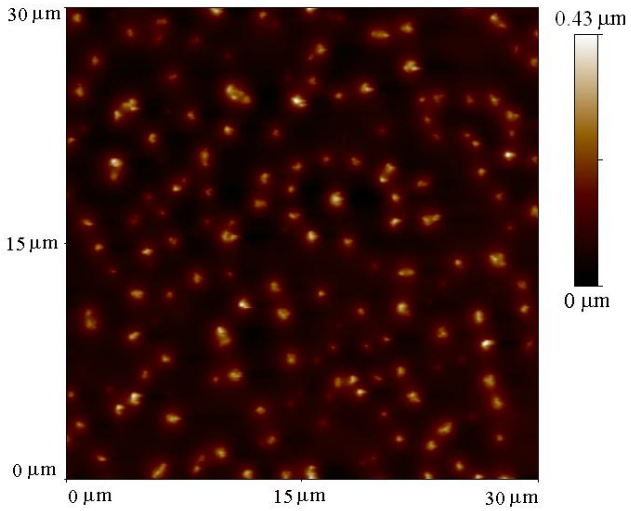

Figure 8. AFM topography scan of a representative PS-C_{60} nanocomposite thin film (h = 135nm) annealed at 180˚C for 30min.

Detailed quantitative analysis of this so-called spinodal clustering morphology has been reported elsewhere [16] and is discussed in terms of a dominant lengthscale λ^* of the spinodal structure and size of individual clusters. The coarsening kinetics of λ^* follows $\lambda^* \sim t^{1/3}$ for relatively thick films (170 nm) and, at longer times, the in-plane structure eventually pins. In addition, the time dependence of the cluster size and number also follows a similar asymptotic behaviour, in comparison to the bulk. The effect of film thickness, matrix molecular weight [16] and annealing temperature [31] are beyond the scope of this paper and will be reported elsewhere, elucidating the underlying mechanism of this spinodal clustering process. The effect of thin film confinement, the presence of a substrate wall and the non-equilibrium solidification process by spin coating might break the symmetry of cluster growth,

leading to the observed clustering behaviour. Lateral diffusion of the NP in polymer nanocomposites thin films is expected to be considerably faster than the vertical diffusion process (i.e., surface attraction/wetting) [32].We interpret this spinodal association behaviour as an interplay between particle-particle clustering and particle-substrate attraction (or 'entropic-push') which is largely governed by a polymer matrix of a given M_w and film thickness. [16].

4. **Concluding remarks**

The stability and structure formation of model polymer-nanoparticle mixtures, such as the present PS-C_{60}, in both bulk and thin films, has significant impact on the function and performance of the nanocomposite system. This work establishes precise conditions for miscibility and characterises the kinetics of the aggregation process in bulk and in confinement. We establish that C_{60} is miscible up to 1-2 % in PS-270k and approximately 160°C based on small angle neutron scattering and calorimetry experiments. In the bulk, coherent scattering intensity grows asymptotically with kinetics described by an empirical rate K, exhibiting Arrhenius dependence. Fractals with a broad range of dimensions D_f ~1.85-2.4 are found, with polydisperse fractal sizes, up to 100s of nm. Confinement in thin films, with thickness ranging from 10-100s of nm, results in symmetry breaking and the emergence of a surface topography with regular spinodal morphology. The wavelength and amplitude of these periodic, interconnected structures can be precisely tuned by the processing parameters temperature, time and concentration. Understanding nanoparticle association and collective self-assembly processes has thus great potential in growing technological applications, particularly in organic photovoltaics and thin film coatings.

References

[1] Balazs A, Emrick T and Russell T P 2006 *Science* **314** 1107.
[2] Mackay M E, Dao T, Tuteja A, Ho D L, Van Horn B, Kim H C and Hawker C J 2003 *Nat. Mater.* **2** 762.
[3] Barnes K A, Karim A, Douglas J F, Nakatani A I, Gruell H and Amis E J 2000 *Macromolecules* **33** 4177.
[4] Holmes M A, Mackay M E and Giunta R K 2007 *J. Nanopart. Res.* **9** 753.
[5] Yaklin M A, Duxbury P M and Mackay M E 2008 *Soft Matter* **4** 2441.
[6] Hoppe H and Sacriciftci N S 2006 *J. Mater. Chem.* **16** 45.
[7] Sariciftci N S, Smilowitz L, Heeger A J, Wudl F 1992 *Science* **258** 1474.
[8] Weng D, Lee H K, Levon K, Mao J, Scrivens W A, Stephens E B and Tour J M 1999 *Eur. Polym. J.* **35** 867.
[9] Mackay M E, Tuteja A, Duxbury P M, Hawker C J, Van Horn B, Guan Z, Chen G and Krishnan R S 2006 *Science* **311** 1740.
[10] Qicong Y, Marecek, J and Chu B 1994 *J. Chem. Phys.***101** 2665.
[11] Zolotukhin I V, Yanchenko L I and Belonogov E K 1998 *JETP Letters* **67** 720.
[12] Martin T P, Naher U, Schaber H and Zimmermann U 1993 *Phys. Rev. Lett* **70** 3079.
[13] Sorensen C M, Oh C, Schmidt P W, Rieker T P 1998 *Phys. Rev. E.* **58** 4666.
[14] Rieker T P, Misono S, Ehrburger-Dolle F 1999 *Langmuir* **15** 914.
[15] Narayanan R A, Thiyagarajan P, Zhu A J, Ash B J, Shofner M L, Schadler L S, Kumar S K and Sternstein S S 2007 *Polymer* **48** 5734.
[16] Wong H C and Cabral J T 2010 *Phys. Rev. Lett.* In press.
[17] Wong H C, Sanz A, Douglas J F and Cabral J T 2010 *J. Mol. Liq.* **153** 79.
[18] Cabral J T 2002 PhD Thesis, Imperial College, London
[19] Sanz A, Wong H C, Douglas J F and Cabral J T 2009 *Submitted*.
[20] Mandelbrot B 1977 *Fractals, Form, Chance and Dimension* (Freeman, San Francisco)

[21] Witten T A and Sander L M 1981 *Phys. Rev. Lett.* **47** 1400.
[22] Witten T A and Sander L M 1983 *Phys. Rev. B.* **27** 5686.
[23] Sander L M, Cheng Z M and Richter R 1983 *Phys. Rev. B.***28** 6394.
[24] Meakin P 1983 *Phys. Rev. Lett.* **51** 1119.
[25] Kolb M, Botet R and Jullien R 1983 *Phys. Rev. Lett.* **51** 1123.
[26] Meakin P 1984 *Kinetics of aggregation and gelation* (New-Holland, New York)
[27] Tuteja A, Duxbury P M and Mackay M E 2007 *Macromolecules*, **40** 9427.
[28] Tuteja A, Mackay M E, Narayanan S, Asokan S and Wong M S 2007 *Nano Lett.***7** 1276.
[29] Alcoutlabi M and McKenna G B 2005 *J. Phys.: Condens. Matter* **17** R461.
[30] Keddie J L, Jones R A L and Cory R A 1994 *Europhys. Lett.* **27** 59.
[31] Wong H C and Cabral J T 2009 *In prepraration*.
[32] Narayanan S, Lee D R, Guico R S, Sinha S K and Wang J 2005 *Phys. Rev. Lett.* **94** 145504.